Power spectral distributions of pseudo-turbulent bubbly flows

S. Mendez-Diaz, J. C. Serrano-García, R. Zenit, and J. A. Hernández-Cordero

Citation: Physics of Fluids (1994-present) **25**, 043303 (2013); doi: 10.1063/1.4800782
View online: http://dx.doi.org/10.1063/1.4800782
View Table of Contents: http://scitation.aip.org/content/aip/journal/pof2/25/4?ver=pdfcov
Published by the AIP Publishing

PHYSICS OF FLUIDS **25**, 043303 (2013)

Power spectral distributions of pseudo-turbulent bubbly flows

S. Mendez-Diaz,[1] J. C. Serrano-García,[2] R. Zenit,[2,a)]
and J. A. Hernández-Cordero[2]
[1]*Facultad de Ingeniería Mecánica y Eléctrica, Universidad Autónoma de Nuevo León, Pedro de Alba s/n, Ciudad Universitaria, San Nicolas de los Garza, 46451 Nuevo León, México*
[2]*Instituto de Investigaciones en Materiales, Universidad Nacional Autónoma de México, México D.F. 04510, México*

(Received 26 June 2012; accepted 22 February 2013; published online 16 April 2013)

An experimental study was carried out to determinate the power spectral density (PSD) of mono-dispersed bubbly flows in a vertical channel using flying hot-film anemometry. To improve bubble detection, optical fibers were installed in close proximity to the anemometer sensing element; in this way, the collisions of bubbles with the probe can be detected and removed from the signal. Measurements were performed with gas fractions up to 6%. The PSD distributions were found to decay with a power of −3, in agreement with previous studies, but for a much wider range of Reynolds and Weber numbers. Our measurements indicate that the power decay does not depend strongly on the nature of hydrodynamic interactions among bubbles.
 [http://dx.doi.org/10.1063/1.4800782]

I. INTRODUCTION

Bubbly flows possess interesting qualities. The motion of bubbles ascending in an otherwise stagnant fluid induce turbulent-like motions in the liquid. However, since the origin of such fluctuating motion is not the same as that from true mono-phasic turbulent flows, these flows are often called pseudo-turbulent.[1] The pseudo-turbulence is very useful for many practical applications. For instance, in bioreactors it is important to have intense mixing to keep the microorganisms active;[2] however, if the agitation level surpasses a certain threshold, cell-lysis can occur.[3] Since agitation induced by bubbles is more "gentle" than that obtained from mechanical impellers, bubble columns are generally preferred. Then to fully utilize the potential of bubbly flows, a complete characterization of the system is needed. One must know the functional dependence of the main variables such as bubble velocity, size, gas volume fraction, agitation, etc. Both experimental[4–7] and theoretical[1] studies have been carried out aiming to determine these relationships for a wide range of Reynolds numbers.

Another interesting feature of the turbulent-like motion observed in bubbly flows is the shape of the power spectral density (PSD) function. Whereas ordinary turbulence shows a −5/3 power decay (the so-called Kolmogorov law) for the inertial sub-range, bubbly flows may present two different trends. Arguably, the trend may be influenced by the value of the bubblance parameter, b, proposed in Ref. 8, defined as

$$b = \frac{0.5\alpha U_R^2}{u'^2_0}, \tag{1}$$

where α, u'^2_0, and U_R are the void fraction, the squared velocity fluctuations (for $\alpha = 0$) and the relative velocity between phases, respectively. With this parameter we can make a distinction between flows in which the fluctuating motion is produced solely by the motion of bubbles (large b), and those

a)Electronic mail: zenit@unam.mx.

in which turbulent fluctuations are already present (small b). If the flow is already turbulent, the addition of bubbles may modify the structure and strength of turbulence and, as a result, modify the power decay of the PSD.

Lance and Bataille[9] were the first to find that the spectral density of energy evolved in a different manner as that observed in classical turbulence. They observed an energy decay close to the power −8/3 and claimed that such a behavior was a feature of bubble-induced turbulence. However, for their investigation the flow was already turbulent, corresponding to values of the bubblance parameter of O(10). For flows with very large b values (i.e., truly pseudo-turbulent flows) different results have been reported. For bubble columns, Mudde *et al.*[10] and Mudde and Saito[11] found a decay exponent close to −5/3. The interpretation of these experimental results must, however, be assessed critically. The shape of the PSD is strongly influenced by the signal processing method (as discussed in detail in Sec. II D); furthermore, shear driven turbulence may have already been present in such investigations since bubble columns tend to be unstable unless very careful alignment and bubble size dispersion measures are taken. On the other hand, the classic −5/3 power decay was observed numerically by Mazzitelli and Lohse,[12] but for the case of point bubbles.

Two recent studies have carefully addressed the experimental and signal processing issues for bubble columns. Riboux *et al.*[13] studied the flow in a bubbly column using a particle image velocimetry (PIV) technique to measure the liquid fluctuations behind the bubble swarm. In this manner, although the intensity of fluctuations was decaying in time, the fluid spectra was calculated without the bubble-interaction problem. They found that the PSD function decayed with an exponent of −3. They also proposed a scaling of the PSD and proposed relevant turbulent-like length scales for these flows. In a similar investigation, using a hotfilm probe, Martinez-Mercado *et al.*[14] found also a −3 decay on the PSD functions. They argued that this behavior was a result of the bubble hydrodynamics, specifically wake effects. Their arguments were based on a comparison with the results of Mazzitelli and Lohse;[12] in their case, the −3 exponent was not observed because their bubbles were small. On the other hand, Risso[15] recently proposed that the −3 exponent is a result of the spatial dispersion of bubbles. Considering a random array of fluid disturbances, he calculated theoretically the PSD and found a −3 power decay. This finding implies that the same PSD decay would be observed in other dispersed two phase flows, regardless if either particles or bubbles were present. The experiments of Amoura[16] seem to confirm this hypothesis. The −3 power decay in the PSD has also been observed for the case of packed beds,[17] further confirming that this behavior is indeed the result of the disperse nature of the bubbles in the flow.

From our point of view, an additional test is needed to close this issue. Bubbly flows can be tested in liquids with different viscosities. In this manner, the nature of the hydrodynamic interactions could be varied as the Reynolds and Weber numbers change. Is the shape of the PSD changed for viscous bubbly flows? Is the −3 power decay preserved? This is the issue that is addressed by this study. We calculate the PSDs for bubbly flows in columns using water and liquids of higher viscosities. We found that for a wide range of conditions the power decay of the PSDs is largely unaffected by the values of the Reynolds and Weber numbers. Our findings are, therefore, in agreement with the predictions of Risso.[15]

II. EXPERIMENTAL ARRAY AND MEASUREMENT TECHNIQUES

The experimental setup is very similar to that used by Martinez-Mercado *et al.*[6] It consists of a vertical acrylic column with a rectangular cross-section of 10×5 cm^2. At the bottom of the column, a bank of capillaries is connected through flanges to a gas chamber. The column was filled with different liquids, water, and water-glycerin mixtures. The physical properties of the liquids used here are listed in Table I. To reduce the amount of coalescence, a small amount of salt ($MgSO_4$, by Aldrich 63138, 99.5% purity) was added to all the liquids.[5]

The mean gas volume fraction, α, was measured from the column hold up, considering

$$\alpha = \left(1 + \frac{H_o}{\Delta H}\right)^{-1}, \tag{2}$$

TABLE I. Physical properties of the test liquids: water and water-glycerin (W-G) mixtures. Morton number: $\text{Mo} = g\mu^4/\rho\sigma^3$.

Liquid (symbol)	ρ (kg/m^3)	σ (N/m^2) ($\times 10^3$)	μ (Pa s) ($\times 10^3$)	Mo ($\times 10^8$)
Water (●) or (○)	998.20	72.04	1.00	2.63
W-G 70-30 (♦) or (◇)	1079.30	66.56	3.35	386.76
W-G 50-50 (□) or (■)	1126.30	64.57	5.58	3134.35

where H_o is the height of liquid without bubbles and ΔH is the increase in height that results after the bubbles have been introduced in the column. For this study, seven values of the gas volume fraction were considered: $\alpha = [0.005, 0.01, 0.02, 0.03, 0.04, 0.05, 0.06]$. The same seven conditions were tested for all cases. For all the results shown here, the initial height H_o was varied to achieve the desired value of volume fraction. The homogeneity of the gas volume fraction within the width of the channel was verified by performing gas volume fraction measurements at several points, as performed by Zenit *et al.*[5] For all the cases tested, the gas volume fraction was found to be uniform, within the experimental uncertainty.

The bank of capillaries was designed following Refs. 5 and 6 to produce a nearly mono-dispersed bubbly flow. To vary the bubble size, two different banks were used. Each capillary bank had capillaries of different internal diameter. A needle valve controlled the flow of nitrogen into the gas chamber onto which the capillary bank was mounted. By varying the Nitrogen flow rate, the gas volume fraction within the columns could be varied. The internal diameters of the capillary tubes used in this study were 0.20 and 1.19 mm to generate small and large bubbles, respectively.

All the measurements conducted in this study are for $b = \infty$. In our case, the liquid velocity fluctuations are the sole result of the motion of the bubbles. Our flows are thus pseudo-turbulent.

A. Single bubble measurements

One of the issues that we aim to investigate is the influence of hydrodynamic interactions among bubbles on the shape of the PSD. Does it make a difference if isolated bubbles rise in rectilinear or oscillatory manner? Do ellipsoidal bubbles induce a different pseudo-turbulent structure than spherical ones?

By changing the size of the bubbles (by having different capillaries) and the fluid properties (using water-glycerin mixtures), we are able to produce different behaviors. We conducted some measurements for single bubbles rising in stagnant fluids using a cylindrical column of 40 cm in height and 8 cm in diameter. The cylindrical container was immersed in rectangular vessel filled with the same liquid, to reduce optical distortion. The bubbles were injected through the bottom using the same two capillaries tube sizes used to build the capillary arrays. The three liquids listed on Table I were used. Nitrogen gas was pumped using a syringe pump considering a very small gas flow rate (about 1 μl/s) such that individual bubbles were produced at a small rate. The motion was filmed with a high speed camera. The results obtained for this set of measurements are summarized in Table II. At least 10 measurements were conducted for each bubble size - fluid combination. The bubble equivalent diameter is calculated from $d_{eq}^3 = d_l^2 d_s$, where d_l and d_s are the long and short axis of the ellipsoidal projection of the bubble, respectively. The bubble aspect ratio is calculated by $\chi = d_l/d_s$.

Clearly, a wide range of parameters can be obtained by varying both the size and the fluid properties; the Reynolds and Weber numbers ranged from 70 to 1000 and from 1.9 to 3.9, respectively. Consequently, the bubbles can ascend either in a rectilinear or oscillatory manner. Figure 1 shows the measured velocities of isolated bubbles for the two capillary sizes used in this study. The measured terminal velocities are compared with the prediction of Moore,[18] which is valid for ellipsoidal bubbles at large Re. The relatively good agreement shows that our experiments are not strongly influenced by surface impurities.

TABLE II. Experimental results for isolated bubbles. For each liquid, two bubbles sizes were produced (two capillary sizes). The letters "O" and "S" correspond to the type of trajectory observed for each bubble, oscillating or straight, respectively. The Reynolds and Weber numbers are defined as $\mathrm{Re} = \rho U_b d_{eq}/\mu$, $\mathrm{We} = \rho U_b^2 d_{eq}/\sigma$, respectively. The superscript "0" refers to isolated bubble conditions.

Liquid (symbol)	d_{eq} (mm)	χ	U_b^0 (mm/s)	Re^0	We^0	Trajectory
Water (○)	3.68	1.93	278.7	1024	3.9	O
Water (●)	1.70	1.57	322.9	550	2.4	O
W-G 70-30 (◇)	3.46	2.06	252.2	374	3.5	O
W-G 70-30 (♦)	1.96	1.52	272.7	229	2.3	S
W-G 50-50 (□)	3.41	1.97	215.1	138	2.7	S
W-G 50-50 (■)	1.97	1.19	188.7	70	1.2	S

B. Measurement of the bubble velocity

The bubble swarm velocity, U_b, was determined with an image processing technique. The flow was filmed with a digital high speed camera which was placed at mid-height of the column. The images were processed with a semi-automatic MATLAB code. A given bubble was identified manually in two consecutive frames (the bubble position was determined by locating three points of its edge). The program calculated the displacement of the bubble center in pixels; since the pixel/mm ratio and the image frame rate were known, the bubble velocity was calculated. A minimum of 300 bubbles were counted for each case to calculate both the mean and variance of the velocity. In this manner, it was possible to obtain accurate measurements of the mean bubble velocity for each size. However, the measurement of the variance has not yet fully statistically converged, so some uncertainty is to be expected.

C. Measurement of the liquid velocity

The liquid velocities were measured with a hot film anemometer (HFA) system. We used a TSI© system (model IFA300). The measuring probe (model 1210-20W) consisted of a

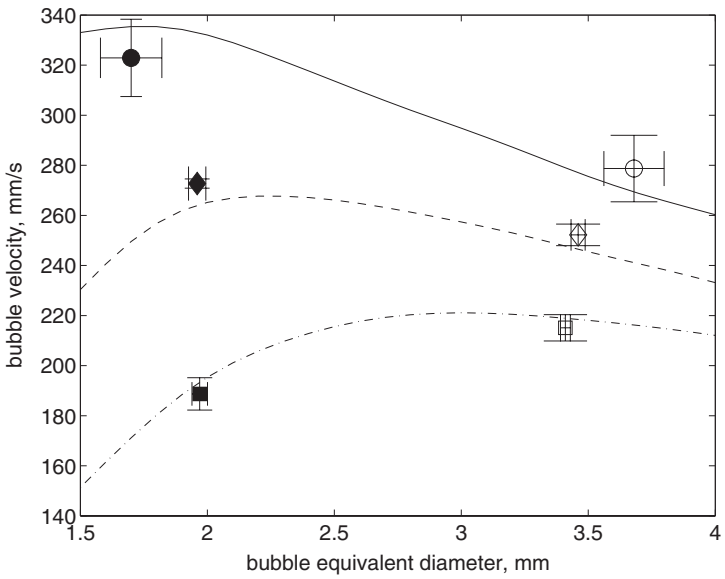

FIG. 1. Terminal velocity of single bubbles as a function of equivalent diameter. The symbols denote experiments conducted in different liquids: (○), water; (◇) water-glycerin 30%; (□) water-glycerin 50%. The filled and empty symbols refer to small and large bubbles, respectively. The lines show the predictions of Ref. 18 for the three liquids used here: (–), $\mathrm{Mo} = 2.6 \times 10^{-8}$; (- - -), $\mathrm{Mo} = 3.9 \times 10^{-6}$; (- · - ·), $\mathrm{Mo} = 3.1 \times 10^{-5}$.

quartz-covered platinum wire. The length of the sensing element is approximately 870 μm and the diameter is 80 μm. The probe is calibrated by displacing the probe at a known translational velocity immersed in a stagnant liquid. The calibration followed the standard fit[19] of $E^2 = A + B V_{trans}^C$ where E was the voltage measured (considering a constant-temperature array) and V_{trans} was the translating velocity; A, B, and C were the constants obtained from the calibration. C had a value close to 1/3 for all liquids, in accordance to previous investigations. For all the measurements an acquisition rate of 15 000 samples/s was considered.

The standard hot-film anemometry cannot be used directly to measure liquid velocities in a bubbly flow because of two main drawbacks. The first one results from the nature of the measurement technique. The sensing element can only measure the velocity magnitude; it cannot determine the flow direction. Hence, reliable results cannot be obtained when the velocity of the liquid is close to zero or when flow reversal occurs. To overcome this limitation, several authors have used "flying" probes.[20,21] In such a case, the probe is moved against the normal direction to the flow to impose a net velocity onto the sensing element. The effect of the probe translational velocity is subtracted during the processing of the signal. We used the system proposed by Martinez-Mercado *et al.*[6] to obtain the liquid velocity measurements. A range of values of V_{trans} was considered. No significant changes in the results were observed as this parameter was modified. For all the results presented here, the translation velocity of the probe was matched with the bubble velocity such that relative velocity between the probe and the bubbles was twice the mean bubble velocity. In this manner we aim to approximately satisfy Taylor's hypothesis.[22]

The second drawback of the hot-film anemometry technique arises from the bubble-probe interaction. When a bubble touches the hot-film sensor, the signal is perturbed due to the different heat conductivity of gas and liquid. This perturbation does not provide useful information and must be eliminated from the signal. Phase identification has been carried out using a threshold method[19] and pattern recognition analysis.[8] Both of these have been implemented through software and the criteria for phase identification are somewhat arbitrary. Furthermore, these methods are only reliable for low void fraction flows.

Phase identification can be significantly improved by using optical fibers, as proposed by Ref. 14. They attached optical fibers placed in close proximity to the HFA probe and bubble interactions are registered via the change in reflectivity at the fiber-end face. Fiber optic probes for bubbly flow analysis have been used by several authors using different shapes in the tip of the fiber. Julia *et al.*[23] studied the pinching effect of the bubble using a conical optical fiber tip in two-phase flows. Bubble detection with these probes depends on the size of the optical fiber and the shape of the bubble, and both of these parameters affect the shape of the signal provided by the probe. Optical fiber probes may yield some additional information, but when combined with the HFA technique, the goal is simply to identify bubble collisions. We implemented this technique in our study, along with the flying HFA. Below, we report the tests that were conducted to characterize this arrangement.

1. Optical fibers as phase identifiers

There are several reports on the use of optical fibers for local measurements of flow parameters such as bubble size or bubble superficial velocity. While a single fiber can be used as a phase identifier in bubbly flows, the use of additional fibers (i.e., multi-probe arrangements) allows to measure other properties such as bubble size, shape, and velocity. Some authors have reported the effect of the shape of the fiber tip on bubble detection[23,24] and several geometries have been used for bubbly flow analysis. Conical fiber tips yield a better performance when detecting the size and shape of the bubbles. In our case, we used cleaved optical fiber tips (i.e., flat fiber end-faces). More recently Vejrazka *et al.*[25] conducted a detailed investigation of the accuracy of optical sensors in bubbly flows. The reader is referred to this reference for detailed discussion in this subject.

A pair of optical fibers attached in close proximity to the hot-film sensor allow to identify the time at which a bubble collides with the sensing element of the hot-film probe. Phase identification is based on the change in reflectivity at the fiber end-face due to Fresnel reflection. The back-reflected signal from a flat fiber tip depends on the difference between the refractive indices of the fiber and the outer medium. Thus, different amplitudes for the reflected signal are expected when the fiber

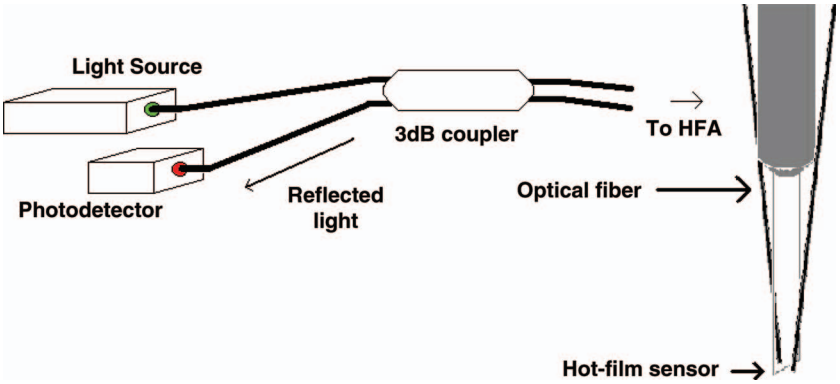

FIG. 2. Optical fiber setup.

is immersed in water or air. In our experiments, the reflected signal increases in amplitude every time that a bubble touches the fiber tip, owing to the reduction in refractive index when a bubble contacts the fiber end-face. The optical setup for detection of the back-reflected signal comprises a light source (a 1550 nm LED) coupled to an optical fiber 3 dB coupler, depicted in Fig. 2. The latter is an optical fiber 50% beam splitter; thus, the output signals from the two fibers of this device are equal in amplitude. The light reflected at the end-faces of either of these fibers is registered via the remaining fiber of the optical coupler, and detection is carried out by a photodetector (1 GHz bandwidth). All the optical fibers used for the optical setup were standard multimode fibers with core/cladding diameters of 62.5/125 μm. The optical fibers were attached to the hot-film sensor with silicone rubber and the separation distance was verified with a microscopic lens mounted in a digital camera. The effective length of the hot-film sensor was less than 1 mm and the distance between the optical fiber and the hot-film probe was less than one bubble diameter. The signal obtained from the optical array was registered with a data acquisition board (National Instruments, model NIPCI60-35E) at 15 k samples/s. Note that having two optical probes greatly increases the detection capacity of the system.

To assess the detection capacity of the optical probes we conducted single bubble experiments, as those shown in Fig. 3. Individual bubbles were released in a small container in which the HFA probe with the optical fibers were immersed. The bubbles were released at different positions such that they collided with the probe in different manners. An effective bubble detection was defined in terms of the so-called piercing position (proposed by Ref. 23) defined as

$$j = \frac{x}{R}, \tag{3}$$

where x is the distance from the bubble center to the tip of optical fiber and R is the maximum horizontal length of the bubble. We tested bubbles of several sizes, the smallest one having $d_{eq} = 1.7$ mm. We determined that, for all cases, a value of the piercing position smaller than 0.95 resulted in a correct detection. Note that our system satisfies the detection schemes proposed by Vejrazka *et al.*,[25] which further corroborates the robustness present experimental array.

The raw signal of the photo detector was converted into a step signal, considering a small threshold value. This signal had either a high or low value if a bubble is detected or not, respectively. This signal was used to remove the bubble collisions in the fluid velocity signal, as described below. Note that the detection scheme was very robust as no significant changes in the shape of the PSD were identified as the step signal threshold was varied slightly.

D. Liquid velocity signal processing

From the step-like signal obtained from the photo detector, the beginning and end of each bubble interaction was determined. From the hot-film signal, the time at which an interaction occurred was

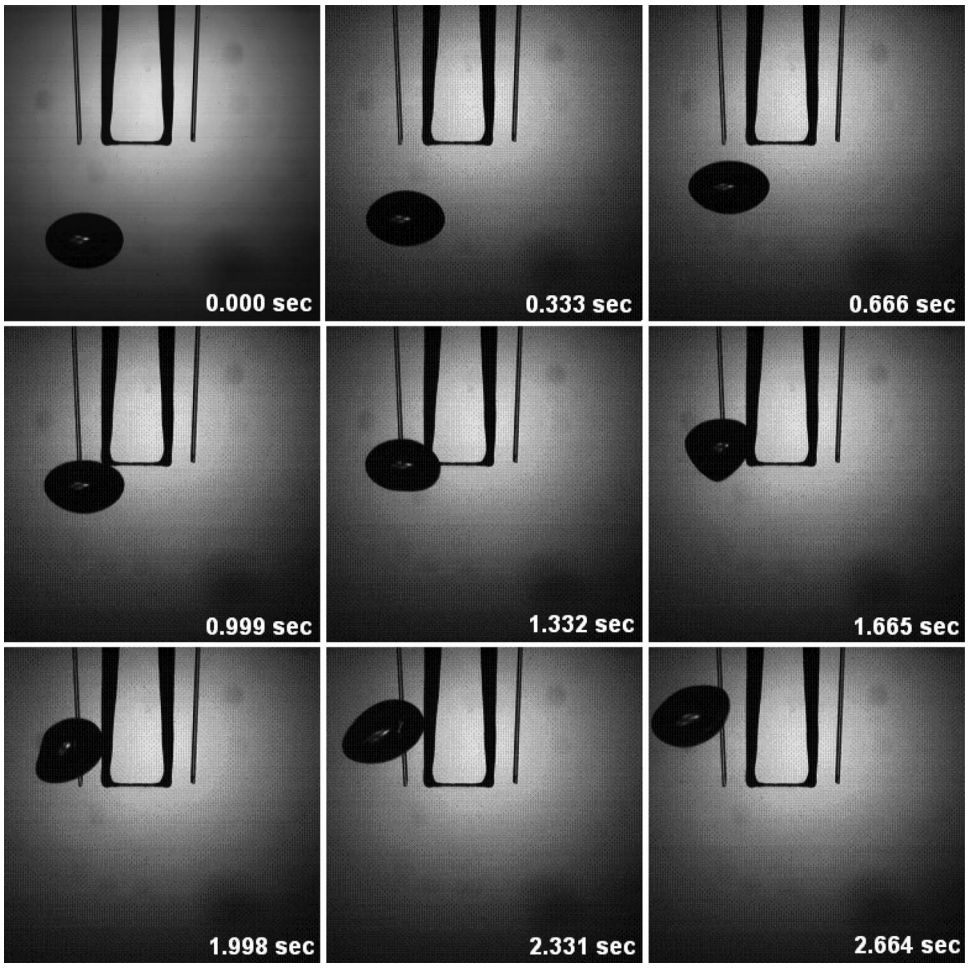

FIG. 3. Bubble collision sequence with both hot-film probe and optical fiber tip. For clarity, in these images the optical probes are shown in the side of the hot-film sensor.

identified and that piece of signal was removed. In this manner many signal pieces without bubble interactions were obtained. These signals were then processed to obtain statistical and spectral results. The liquid velocity fluctuations were calculated directly as the variance of the entire set of signal pieces. For each measurement, at least 8 measurements were conducted, i.e., the probe was traversed 8 times. The duration of each measurement varied depending on the speed of the probe; the minimum total measurement time (for the fastest bubbles) was approximately 2 s, for each traverse test.

The following procedure was adopted to calculate the PSD function for each flow condition. The spectral density was calculated for each piece of the signal (where no bubble collisions occurred) using Welch's method.[26] The mean spectral density was calculated by averaging the PSDs of each trace. Since the length of each signal was different, the range of frequencies was different for all cases, in particular for the low frequency end of the range. The data for lower frequency had to be adjusted by these variations in event occurrence.

It is important to note that we had to adopt a criteria to discard signal pieces that were shorter than a certain minimum length. During the initial processing of these data, we noted that the shape of the PSDs varied significantly if all signals were included. In particular, when the gas fraction was large (high collision rates), we had many short-length signals. We argue that such short signals add spurious components to the PSD, specially in the low frequency range because they do not contain enough information. To further investigate this issue we conducted a series of additional experiments in a different setup. We obtained well-characterized measurements of a single-phase turbulent flow.

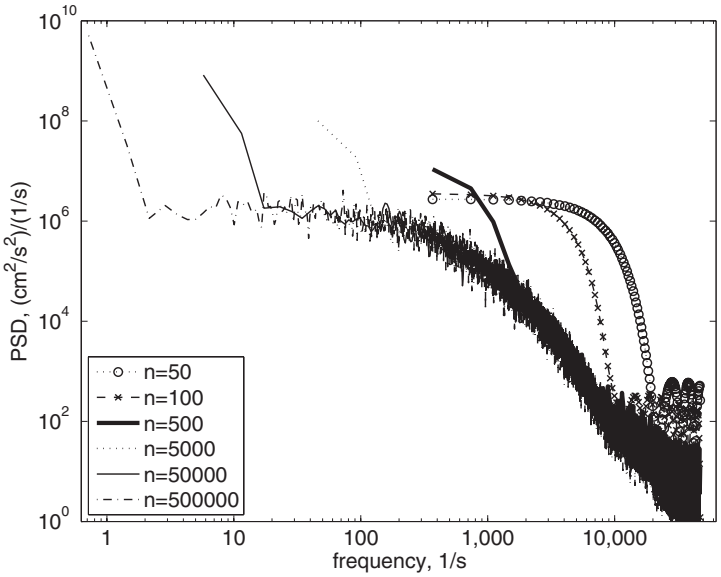

FIG. 4. Effect of the signal length on the shape of the PSD. The signal length, n, is defined by the number of data points of the total sample, acquired at 15 000 samples per second. Each line represents the average power spectral distribution obtained for different values of n.

Using an isotropic turbulence chamber,[27] a continuous fluctuating velocity signal was obtained using the hot film probe. For this test, the liquid did not contain bubbles. The PSD of the entire signal (500 000 data points) was obtained. This result is shown in Fig. 4. In this case, the typical $-5/3$ power law decay is observed for high frequencies. Then, this signal was broken into shorter pieces, varying the signal size from 50 to 100 000 data points. The PSD was calculated for each piece and from all the PSDs an average spectra was obtained (following the procedure described above). The averaged PSD for each case of signal length is shown in Fig. 4. It is clear that if the signal length is longer than a certain threshold, the shape of the PSD is preserved; as the signal becomes shorter, the low frequency components disappear, but the energy decay at high frequency remains unchanged. When the signal is shorter than 500 data points, the shape is significantly different. First, the lowest frequency for which the PSD can be calculated is much higher; hence, the low frequency behavior is lost. Most importantly the PSD, for such short data sets, is nearly flat; the energy decays only as the frequency approaches the Nyquist value. This is an indication that the velocity fluctuations are no longer correlated (the PSD of white noise would not depend on frequency). This change of trend for short data sets indicates that such signals should be discarded to calculate the PSD. Clearly, with this test we established a criteria to eliminate short signals for the case of velocity traces obtained from the bubbly flow.

The signal length threshold can be justified as follows. A characteristic sampling time can be defined as $T_c = \lambda/U_b$, where U_b is the bubble velocity and λ is the mean uniform distance between bubbles. If we assume that the bubbles are randomly distributed in space, we can calculate λ as, $\lambda = N^{-1/3}$ where N is the number of bubbles per unit volume (bubble number density). Since the gas volume fraction can be written in terms of the bubble number density ($\alpha = N\pi d_b^3/6$), the characteristic time can be written as

$$T_c = \left(\frac{\pi}{6}\right)^{1/3} \frac{d_b}{U_b \alpha^{1/3}}. \tag{4}$$

This time represents the mean time between bubble collisions. Therefore, in average, we must have sample length that considers, at least, this time period to effectively capture liquid velocity fluctuations. Considering the sampling frequency of our hot-film system, f_{AQ}, we can calculate the most appropriate number of points in a series, n, to calculate the PSD,

$$n = f_{AQ}\lambda. \tag{5}$$

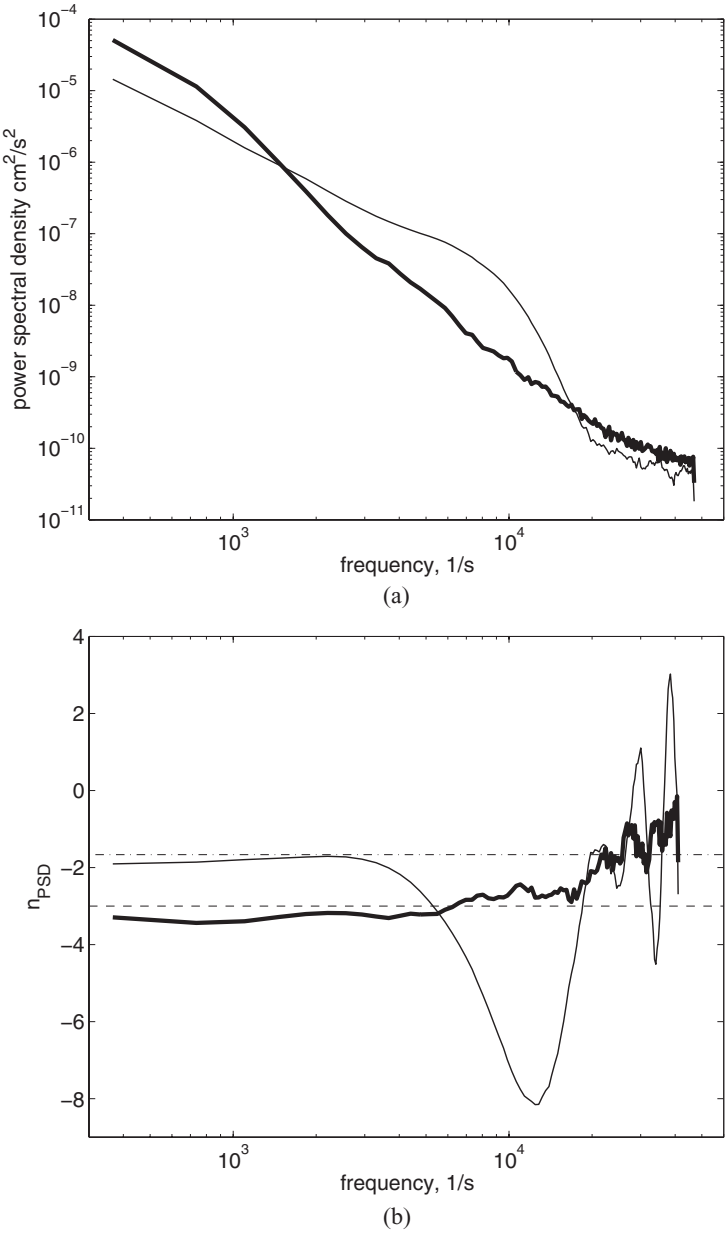

FIG. 5. (a) Power spectral density: Spectral distribution obtained with and without length validation criteria, thick and thin lines, respectively. (b) Power decay: Rate of decay of the PSD, n_{PSD}, as a function of frequency with and without length validation criteria, thick and thin lines respectively. The horizontal lines show the classical -3 (dashed line) and $-5/3$ (dashed-dotted line) values of n. For the case shown here $d_b = 4.7$, $\alpha = 5\%$, $Re = 342$, and $We = 3.2$.

For the type of experiments conducted in this investigation, the smallest characteristic time is given by the highest volume fraction and faster velocities. Considering the case of a 2 mm bubble, moving at 300 mm/s at a gas volume fraction of $\alpha = 0.005$, we calculate that $n = 470$. For all other cases, n is higher. Therefore, a sample length of about 500 data points should contain enough information to correctly capture the temporal correlation of fluid velocity fluctuations.

As an example, Fig. 5(a) shows the average spectral density calculated from a typical signal obtained from the flying hot-film probe with phase identification. The spectral density was calculated in two different ways. First, the PSD was calculated considering all the signal segments obtained after removing the bubble-probe interaction detected by the optical fibers. Then, the PSD was calculated

again considering a signal length threshold of $n = 500$ data points, i.e., all signals shorter than 500 data points were discarded. Evidently, the effect of including a signal length discrimination criteria is very significant: the shape of the PSD changes drastically. Note that all PSD curves in this investigation are expressed in SI units (Hertz are converted in 1/s considering a factor of 2π). Note also that the number of pieces discarded by this scheme increases with gas volume fraction and it can be as large as 12% of the entire data set for the highest gas fraction. However, we did not observe a significant effect of the amount of discarded signals in the shape of the obtained PSDs, but some loss of statistical convergence may be expected as the total measuring time is reduced by the filtering scheme.

Finally, since we are particularly interested in the rate of decay of the PSD with frequency, we measured it considering the following scheme. For each frequency, a portion 15 data points (forward) were used to obtain a fit of the form $\text{PSD} = Af^{(n_{PSD})}$. Figure 5(b) shows the fitted value of n_{PSD} as a function of frequency for the data shown in Fig. 5(a). Clearly, for the case in which the length threshold is adopted, the power decay of the signal is close to -3 for the entire frequency range. Note that the number of points chosen to find this fitting was chosen arbitrarily: smaller data samples resulted in noisier curves (than those shown in Fig. 5(b)); larger data sets, reduced the range of frequencies shown in the plots. However, the trends are preserved for data sets as small as 5 data points.

III. RESULTS

Figure 6 shows images of monodisperse flows obtained with our setup. It is evident that the flows are nearly monodispersed. As the viscosity of the liquid increases, the shape of the bubbles becomes less deformed. For all flow conditions, the bubble diameter was observed to slightly increase with gas volume fraction. For instance, for water and the small capillaries, the bubble diameter for very

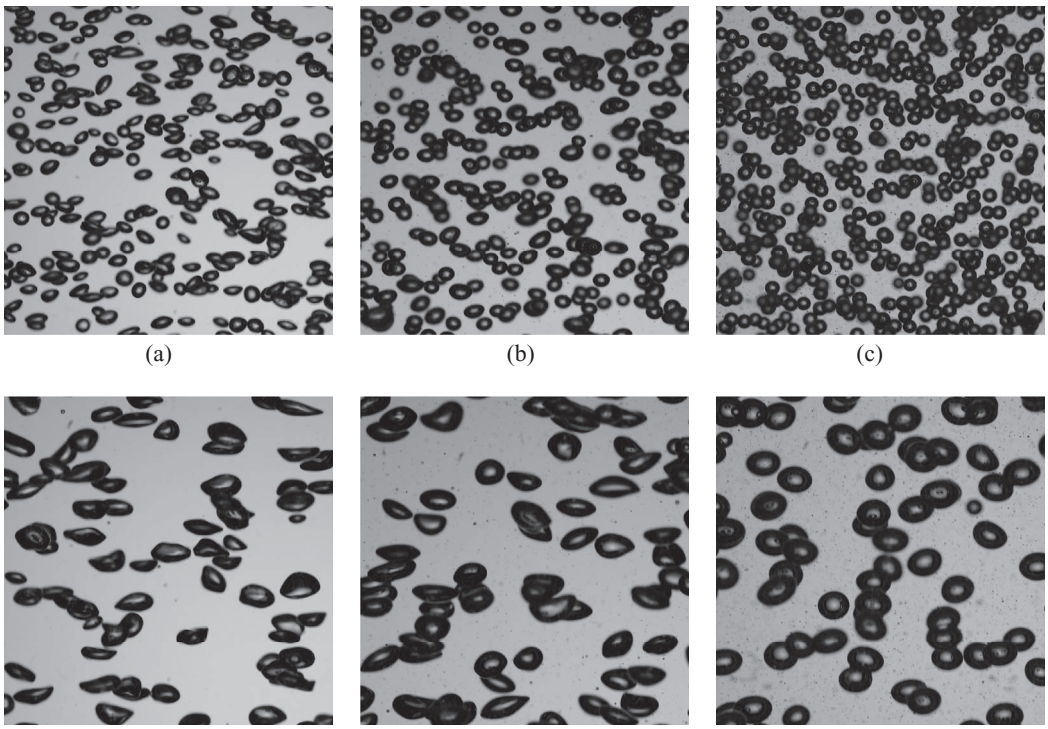

FIG. 6. Typical mono-dispersed bubbly flows. Images obtained for different liquids for a gas volume fraction of $\alpha = 0.02$. The top and bottom rows show images obtained for the small and large capillary array, respectively. Water, (a) and (d); water-glycerin (70-30), (b) and (e); water-glycerin (50-50), (c) and (f). The size of each image is approximately 5×5 cm^2.

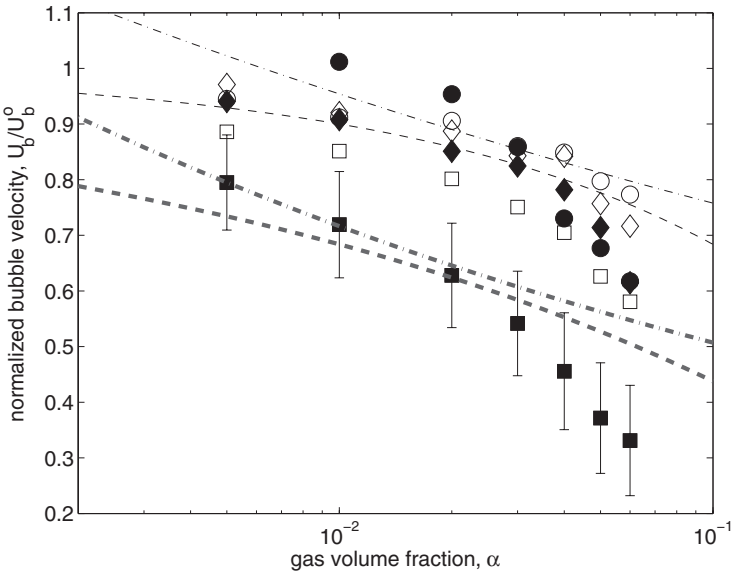

FIG. 7. Normalized bubble velocity as a function of gas volume fraction, for monodisperse flows. The symbols denote experiments conducted in different liquids: (○), water; (◇) water-glycerin 30%; (□) water-glycerin 50%. The filled and empty symbols refer to small and large bubbles, respectively. The dashed and dashed-dotted lines represents the fits from Eqs. (6) and (7), respectively; the thick and thin lines show the fits for the highest ($A = 0.49$ and $B = 0.1$) and smallest Reynolds number experiments ($A = 0.25$ and $B = 0.15$), respectively. For clarity, only one set of data shows typical error bars.

dilute flows ($\alpha < 0.005$) grew from $d_b = 1.97$ mm to $d_b = 2.55$ mm when the gas volume reached a value of $\alpha = 0.06$ (about a 30% increase in size). The same amount of increase was observed for all cases.

Figure 7 shows the normalized bubble velocities as a function of gas volume fraction for all flows studied here. The normalization is obtained considering the single bubble velocity, U_b^o, for each case (see Table II). In all cases, the mean bubble velocity is observed to decrease with gas volume fraction, in accordance with many previous measurements.[5,6] As shown in the figure, the hinderance of bubble velocity is stronger as the Reynolds number decreases. For large Reynolds numbers, the dependance of the bubble velocity on the gas volume fraction agrees well with the expression proposed by Ref. 13:

$$U_b = U_b^o(1 - \alpha^A), \tag{6}$$

where $A = 0.49$. A reasonable agreement can be observed for the whole range of gas volume fractions tested here ($0.005 < \alpha < 0.06$) for large bubbles in water ($Re_o = 1024$). Similarly, Riboux *et al.*[13] proposed a different fit to resolve the apparent discontinuity on the bubble velocity for $\alpha \to 0$ that Martinez-Mercado *et al.*[6] reported. The fit

$$U_b = U_b^* \left(\frac{\alpha^*}{\alpha}\right)^B, \tag{7}$$

where $B = 0.1$, $\alpha^* = 0.005$, and $U_b^* = 32.5$ cm/s, also appears to fit the data reasonably well for the large bubbles in water for $\alpha > 0.01$. However, for smaller Reynolds numbers these fits do not agree well with the experimental measurements. For the experiments for the small bubbles in the 50-50 water-glycerin fluid (the smallest Reynolds number), the fits were attempted considering $A = 0.25$, $B = 0.15$, $\alpha^* = 0.005$, and $U_b^* = 15.0$ cm/s. As shown in Fig. 7, the agreement is not very good. Clearly, the change in Reynolds and, possibly, Weber numbers affect the nature of the hydrodynamic interactions and, therefore, affect the behavior of the ascending bubbly flows.

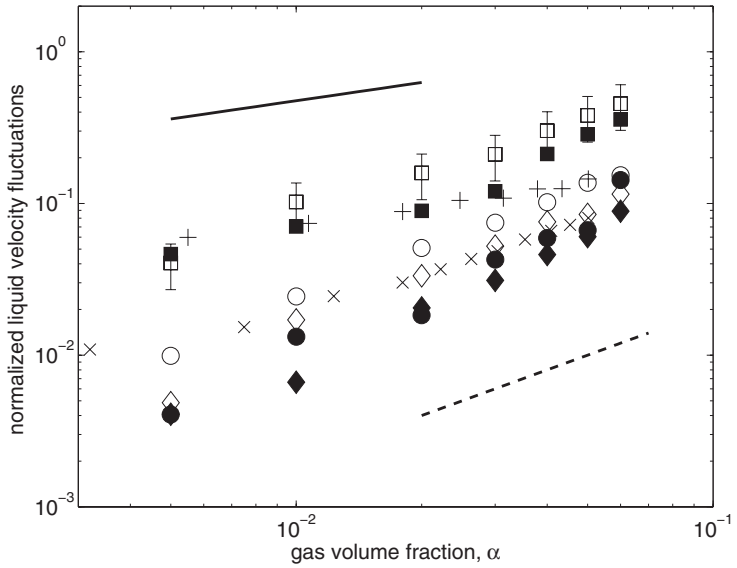

FIG. 8. Normalized liquid velocity variance as a function of gas volume fraction, α. All symbols are the same as in Fig. 7. The (+) and (×) symbols show experiments from Martinez-Mercado *et al.*,[6] for which (Re,We) are (500,1.7) and (200,2.0), respectively. The lines show trends of the form $T_l \sim \alpha^C$: continuous line, $C = 0.4$; and dashed line, $C = 1.0$. For clarity, only the (□)-data show error bars.

A. Liquid velocity variance

Figure 8 shows the measured liquid velocity variance as a function of the gas volume fraction for all the cases tested in this investigation. The variance is normalized by considering the mean bubble velocity for the corresponding bubble-liquid and gas volume fraction combination. Hence, the normalized liquid velocity fluctuation is defined as

$$T_l = \frac{\langle U_l'^2 \rangle}{U_b^2}. \tag{8}$$

In all cases, the fluid fluctuations increase with gas volume fraction. As the Reynolds number decreases, the normalized liquid velocity fluctuations increase. These two main features of T_l are in good agreement with the measurements of Ref. 6 for the similar values of the Reynolds and Weber numbers. Furthermore, the measurements show that for experiments with large *Re* the liquid fluctuations increase linearly with gas volume fraction; this tendency is expected considering inertial hydrodynamic interactions (see Refs. 1 and 6). On the other hand, for flows with Re of O(10) the normalized liquid velocity fluctuations increase at a smaller rate with gas volume fraction, again, as previously shown by Refs. 4, 6, and 7. Once again, this change of behavior is a result of the modification of the flow dynamics resulting from the reduced Reynolds number.

As an additional test to further verify that the length discrimination scheme did not affect the validity of our results, the value of the fluid velocity variance was also calculated by considering that

$$\langle U_l'^2 \rangle = 2\pi \int_0^\infty PSD(f) df.$$

We found that the values of $\langle U_l'^2 \rangle$ could be obtained correctly in this manner, in good agreement with the results shown in Fig. 8. Both the order of magnitude and trend could be reproduced in all cases. However, some important differences were observed for gas volume fractions higher than 4%. The differences in the measurements could be attributed to the limited frequency range that could be attained by the present experimental setup. Nevertheless, this test corroborates that the filtering of shorter signals does not modify the character of the measurement in a significant manner.

B. Mean fluid spectra

As shown above, the behavior of the mean bubble and fluctuation liquid velocities show a different behavior as the inertia of the flow decreases. The main issue that we want to address in this investigation is what is the effect of decreasing inertia in the shape of the power spectral density of the liquid velocity signal. Note that all spectra are shown in SI units, both in frequency and spectral power.

First, we show results for a typical case in which only the gas volume fraction is varied considering only one liquid and one bubble size. Figure 9(a) show the PSDs for the 70-30 water-glycerin, for large bubbles ($d_b \approx 3.4$ mm). We observe that the spectral power decays with

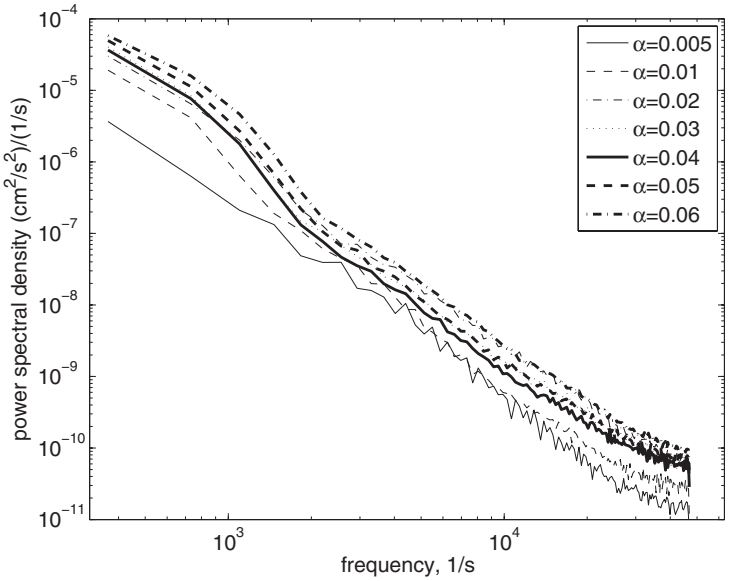

(a)

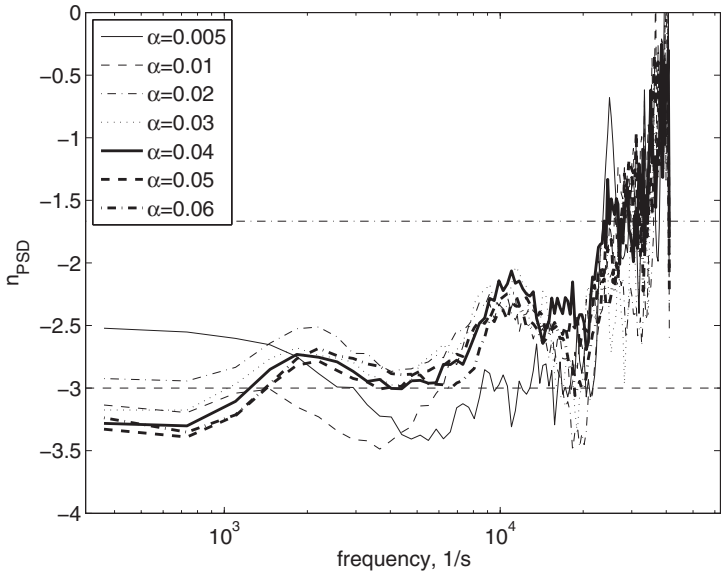

(b)

FIG. 9. Variation of PSD with gas volume fraction. (a) Power spectral density: spectral distribution; (b) power decay: rate of decay of the PSD, n_{PSD} as a function of frequency. The horizontal lines show the classical -3 (dashed line) and $-5/3$ (dashed-dotted line) values of n_{PSD}. The liquid used in this case was the 70-30 water-glycerin solution; the bubble size is $d_b \approx 3.4$ mm.

frequency, as expected. The energy involved in the liquid fluctuations increases as the gas volume fraction increases, in agreement with the results shown in Fig. 8.

As shown clearly in Fig. 9(b), the energy decay exponent is close to −3 for all cases, up to frequencies of 3000 1/s. For frequencies larger than 4000 1/s, the decay exponent of the PSDs, in all cases, is closer to a value of −5/3. We can argue, then, that at small scales, corresponding to large frequencies, the liquid fluctuations behave in a manner similar to that of ordinary turbulence in the inertial subrange. For larger scales, the liquid fluctuations mostly result from a different mechanism. Risso[15] recently showed that a decay exponent of −3 is expected for fluctuations resulting from a disordered array of bubbles.

Figure 10 shows the PSDs and the fitted values of n_{PSD} as a function of frequency for experiments conducted at a fixed value of gas volume fraction, $\alpha = 0.02$, varying the liquid used and the bubble size. For low frequencies, the energy associated with liquid fluctuations is larger for the cases showing the experiments with the smallest Reynolds numbers, in agreement with the results shown in Fig. 8; however, for higher frequencies the trend changes and it is not monotonic. Nevertheless, it is very clear that for all cases the decay exponent is very close to −3 for frequencies smaller than 1000 1/s. For frequencies larger than 3000 1/s, the decay exponent is much closer to the classical −5/3 value. It is remarkable that this behavior is largely unaffected by the values of the Reynolds and Weber numbers.

Finally, to further demonstrate the robustness of the −3 value of the decay exponent, in Fig. 11 we show the PSDs of all the experiments conducted in this study. These results include the measurements obtained for the three different liquids, the two bubble sizes and the seven values of the gas volume fraction. All results show the same general trend: at small frequencies, the energy of the PSD decays according to a −3 power; for large frequencies, the decays is closer to the −5/3 power. Evidently, the magnitude of the PSD change as the Re, We and gas volume fraction are varied. However, the way in which the energy is transferred from large to smaller scales is very similar for all cases. Therefore, we can argue that the nature of the hydrodynamic interactions does not play a significant role in the organization of liquid velocity fluctuations for bubbly flows. As a comparisons, a measurement from Martinez-Mercado *et al.*[14] is shown along our measurements. Although a direct comparison is not possible (they used arbitrary units for the PSD), the agreement in the trend is very clear; a slight difference can be identified: for their measurements the decay rate is reduced at lower frequencies.

C. Characteristic length scales of fluctuating motion

From the results shown above, it is clear that the power decay of the PSDs is closer is −3 for small frequencies and that in all cases, the decay evolves to −5/3 for larger frequencies. It is therefore interesting to calculate the length scales of the turbulent-like motion of these flows.

Following Tennekes and Lumley,[28] the Kolmogorov length scale, η, can be calculated as

$$\eta = \left(\frac{\nu^3}{\epsilon}\right)^{1/4}, \tag{9}$$

where ν and ϵ are the kinematic viscosity and the dissipation rate, respectively. Hence, the value of ϵ must be known to infer η. Riboux *et al.*[13] used the rate of decay of turbulent kinetic energy behind the bubble swarm to calculate ϵ. In our case, we cannot use the same scheme because our flows are continuous. In turn, the energy dissipation rate can be calculated by considering the second-order structure function of the flow, S_2.[29] Considering that the Taylor hypothesis is valid, as discussed in Sec. II C, the time dependence of the signal can be interchanged by a spatial dependence: $x = t V_{mean}$, where V_{mean}, in our case, would be the displacement velocity of the probe (since our flows are pseudo-turbulent, $V_{mean} \approx 0$).

The second-order structure function is defined as

$$S_2(X) = \langle (V(x+X) - V(x))^2 \rangle, \tag{10}$$

where $V(x+X) - V(x)$ is the velocity difference function and X denotes the separation distance between two points in space. The brackets denote statistical average. Now, it can be shown that the

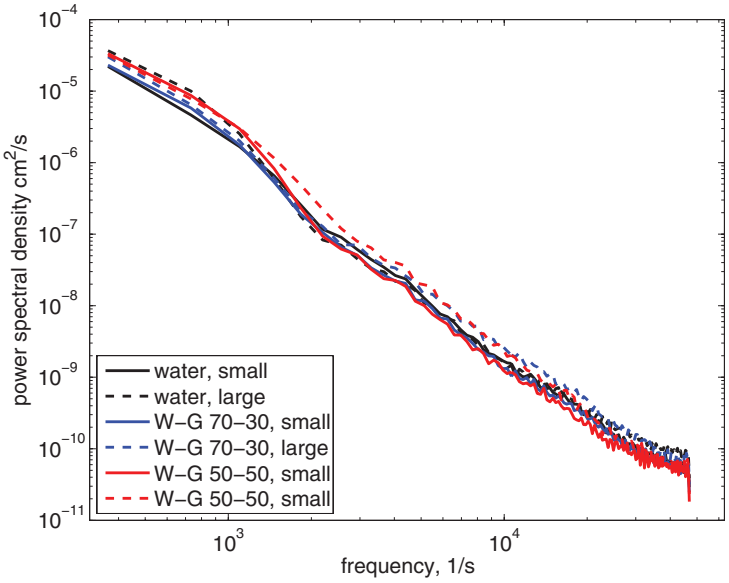

(a)

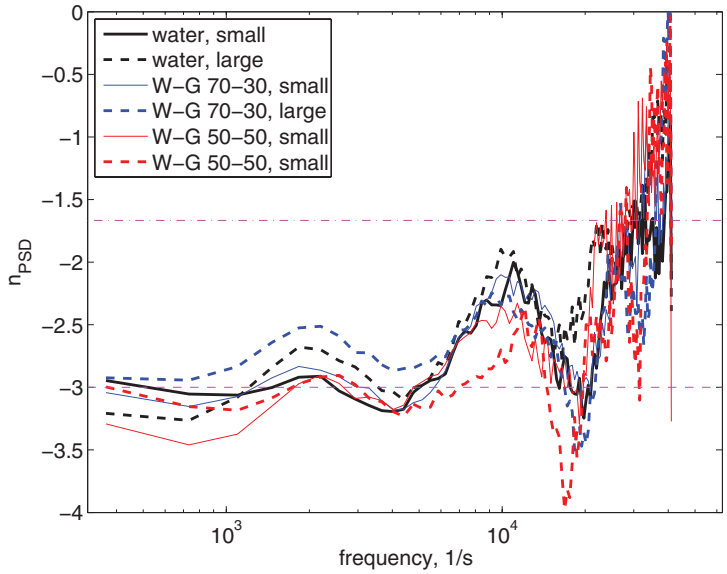

(b)

FIG. 10. Variation of PSD with liquid viscosity and bubble diameter. (a) Power spectral density: spectral distribution; (b) power decay: rate of decay of the PSD, n_{PSD}. The horizontal lines show the classical -3 (dashed line) and $-5/3$ (dashed-dotted line) values of n. A gas volume fraction of $\alpha = 0.02$ was used for all the cases.

structure function scales as

$$S_2(X) = C_2 \epsilon^{2/3} X^{2/3}, \tag{11}$$

where $C_2 = 2.13$, is a universal constant. From our velocity signals it is straightforward to calculate S_2. The value of ϵ is calculated by locating the plateau-value of the function $S_2(X)X^{-2/3}$ for intermediate values of X.

We found that the η is smaller than the bubble size by a factor of about 10 for all scales and that it decreases monotonically with gas volume fraction. The size of η and its decrease with α are features which are in very good agreement to those reported by Riboux *et al.*[13] Furthermore, we found that η increases with the viscosity of the fluid, as one may expect.

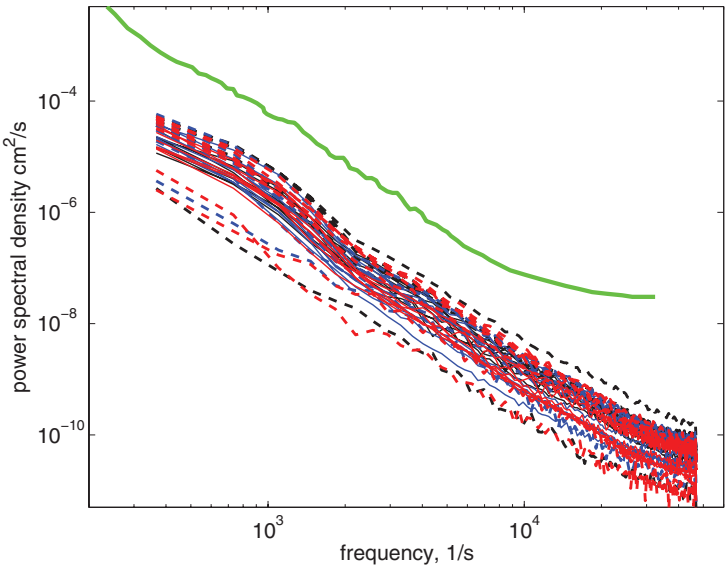

(a)

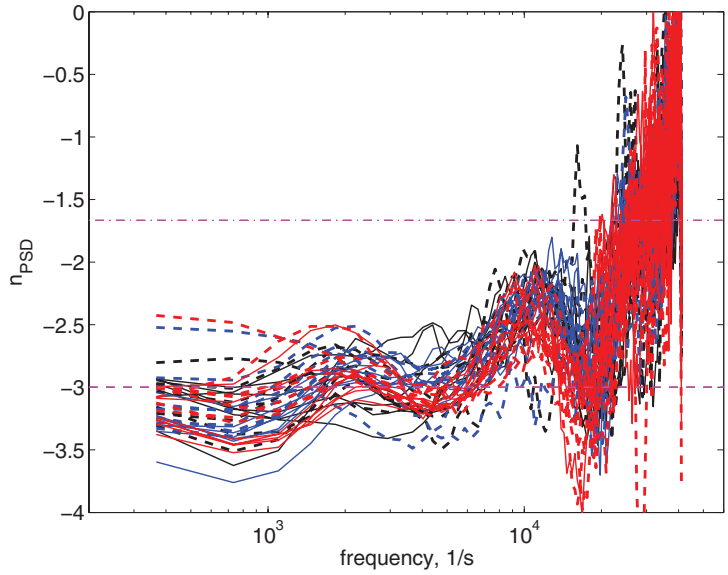

(b)

FIG. 11. PDF of liquid velocity for all cases tested here. The black, blue and red lines show the results for water, W-G 70-30 and W-G 50-50 mixtures, respectively. The continuous and dashed lines show the results for small and large bubbles, respectively. (a) PSD and (b) power decay. The green thick line show a typical result from Ref. 14.

Therefore, one may expect that small scales, and their corresponding high frequencies, the fluctuating motion is closer to that observed in ordinary turbulence.This fact would explain why the $-5/3$ power decay is recovered for higher frequencies. It is important to emphasize that the calculations presented here correspond to a state of homogeneous turbulence. The fluctuating nature of the bubbly flows discussed here is different from grid-generated turbulence. Therefore, these estimations must be considered only crude approximations.

D. Scaling of fluid spectra

Finally, we attempt a normalization of the spectra obtained in this study. First we consider the scheme proposed by Riboux *et al.*[13] They normalized the PSD by the liquid velocity variance, $\langle U_l'^2 \rangle$

and a characteristic length scale formed by $(U_b^o)^2/g$. In our case, since we calculate the spectra from a time series, the equivalent time scale is U_b^o/g. Therefore

$$PSD^* = \frac{PSD}{\langle U_l'^2 \rangle} \frac{U_b^o}{g}. \tag{12}$$

Instead of the wave length, the frequency, therefore, can be normalized as

$$f^* = \frac{f U_b^o}{g}. \tag{13}$$

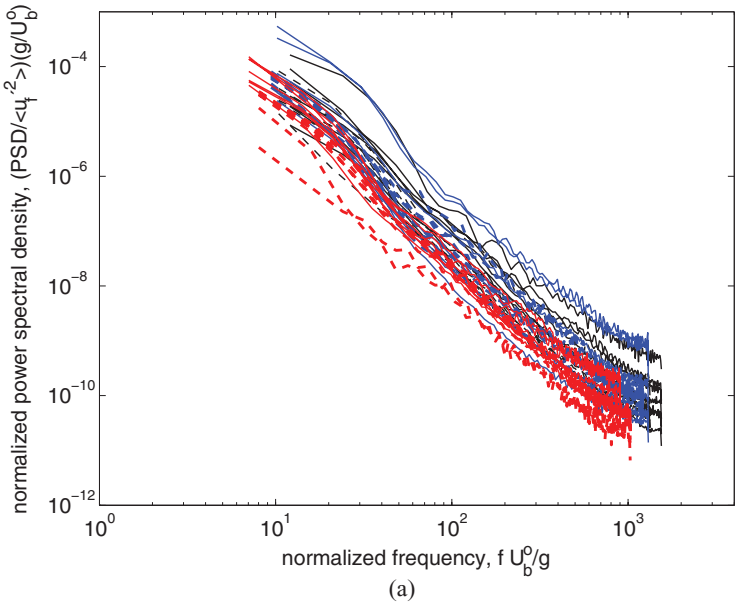

(a)

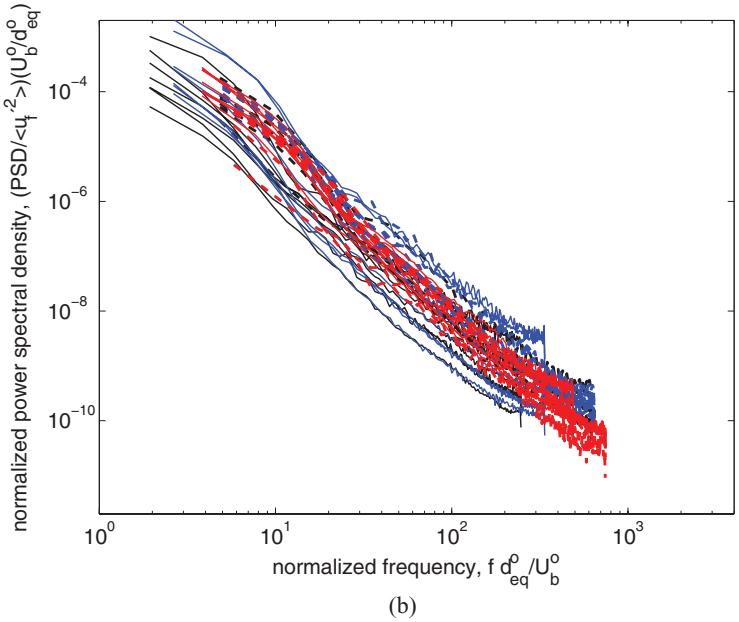

(b)

FIG. 12. Normalized PDF of liquid velocity for all cases tested here. The black, blue, and red lines show the results for water, W-G 70-30 and W-G 50-50 mixtures, respectively. The continuous and dashed lines show the results for small and large bubbles, respectively. (a) and (b) show normalization proposed by Ref. 13 (Eqs. (12) and (13)) and that proposed here (Eqs. (14) and (15)).

All the spectra calculated in this study, considering this normalization are shown in Fig. 12(a). It is not clear if the normalized PSDs are closer in magnitude, but the dispersion is reduced somehow. In particular, the data for the more viscous fluid appear to deviate from the other two less viscous cases.

Next we consider a different time scale for the normalization. If we consider d_{eq}^o/U_b^o, the normalization of PSD and frequency are

$$PSD^* = = \frac{PSD}{\langle U_l'^2 \rangle} \frac{d_{eq}^o}{U_b^o}, \tag{14}$$

$$f^* = = \frac{f d_{eq}^o}{U_b^o}. \tag{15}$$

The spectra, normalized considering this scheme, is shown in Fig. 12(b). As in the previous case, the normalization does not collapse the data into a narrow region. The spread of the data is slightly smaller than in the previous case. In this case, the data for the different fluids is not distinctively separated from one another.

IV. FINAL COMMENTS AND CONCLUSIONS

In this investigation we have conducted measurements of the liquid velocity signal in pseudo-turbulent flows ($b = \infty$). The main objective of these measurements was to discern the effect of varying the nature of hydrodynamic interactions on the shape of the power spectral density. As discussed in the Introduction, a power decay close to -3 had been observed for many bubbly flows. However, all of the previous studies considered air-water systems for which the Reynolds and Weber numbers cannot be varied widely for milimetric size bubbles. We have used two different bubble sizes and three liquids to change significantly the nature of the flow around the bubbles. Despite these efforts we found that, for all cases, the PSDs of the pseudo-turbulent bubbly flows decay with an exponential slope close -3, closely to what was found previously.

So, the main conclusion of our investigation is that the specific details of the hydrodynamic interactions among bubbles do not influence that way in which the pseudo-turbulent fluctuations are produced. This peculiar agitated state must, therefore, be a result of disorder of the bubble array. Risso[15] recently calculated the PSD for a simple 1D case, in which the bubbles were randomly distributed in space. He found that for an intermediate subrange the PSD decayed as the power -3 of the wave number. Our results, therefore, support the idea that the liquid velocity fluctuations arise mainly from bubble distribution and not so much from the hydrodynamic interactions. In fact, Risso argued that the details of the distribution did not have a significant effect of the shape of the PSD; this idea is also in agreement with our results. Clearly, if the flow is more or less viscous, the bubbles will be dispersed in a different manner in the liquid. Regardless of the specific details of the dispersion, the PSD remains largely unaffected. This fact is very interesting; it implies that the way in which the liquid motion is organized in space does not depend on the prevalence of inertial, viscous, or surface tension effects.

On the other hand, we could not find a definite normalization scheme for the PSD. We showed that the normalization scheme proposed by Riboux *et al.*[13] did not successfully scaled the PSD for all cases. The arguments that they used were based on the variation of mean bubble velocity and liquid velocity fluctuations of the bubble ensemble. As shown in Fig. 7, the functional dependence that they proposed is not appropriate for more viscous flows. Hence, it is not surprising that their normalization scheme failed for a different range of Reynolds numbers. Likewise, we found that the liquid velocity fluctuations increase linearly with gas volume fraction for water-air systems; the dependence is weaker for more viscous liquids. We propose an alternative time scale to normalize the PSDs. By considering the bubble characteristic time, d_{eq}^o/U_b^o, but preserving the mean fluctuating liquid velocity, a normalization was attempted. Although it is not clear that this choice is more effective than that of Riboux *et al.*, a trend depending on the Reynolds number is not discernible.

If this scaling is considered correct, it would imply that the local hydrodynamic state around the bubble is important for wide range of scales.

This result is valid for pseudo-turbulent flows, that is, flows in which the liquid fluctuations are the sole result of the presence of bubbles. It would be interesting to conduct similar analysis for turbulent flows which contain bubbles. In such a way, it could be possible to assess when each effect would dominates the organization of liquid motion in the flow: spatial inhomogeneity or ordinary turbulent energy cascade. We plan to pursue studies in this direction in the future.

ACKNOWLEDGMENTS

S.M.-D. acknowledges the support of the DGAPA-UNAM through its postdoctoral scholarship program. J.C.S.-G. is grateful to DGEP-UNAM for financially supporting his graduate studies.

[1] L. van Wijngaarden, "On pseudo turbulence," Theor. Comput. Fluid Dyn. **10**, 449 (1998).
[2] N. Kantarci, F. Borak, and K. O. Ulgen, "Bubble column reactors," Proc. Biochem. **40**, 2263 (2005).
[3] Y. Chisti, "Hydrodynamic damage to animal cells," Crit. Rev. Biotechnol. **21**, 67 (2001).
[4] A. Cartellier and N. Riviere, "Bubble-induced agitation and microstructure in uniform bubbly flows at small to moderate particle Reynolds numbers," Phys. Fluids **13**, 2165 (2001).
[5] R. Zenit, D. L. Koch, and A. S. Sangani, "Measurements of the average properties of a suspension of bubbles rising in a vertical channel," J. Fluid Mech. **429**, 307 (2001).
[6] J. Martinez-Mercado, C. A. Palacios-Morales, and R. Zenit, "Measurement of pseudoturbulence intensity in monodispersed bubbly liquids for $10<\mathrm{Re}<500$," Phys. Fluids **19**, 103302 (2007).
[7] A. Cartellier, M. Andreotti, and P. Sechet, "Induced agitation in homogeneous bubbly flows at moderate particle Reynolds number," Phys. Rev. E **80**, 065301(R) (2009).
[8] J. Rensen, S. Luther, and D. Lohse, "The effect of bubbles on developed turbulence," J. Fluid Mech. **538**, 153 (2005).
[9] M. Lance and J. Bataille, "Turbulence in the liquid phase of a uniform bubbly air-water flow," J. Fluid Mech. **222**, 95 (1991).
[10] R. F. Mudde, J. S. Groen, and H. E. A. van den Akker, "Liquid velocity field in a bubble column: LDA experiments," Chem. Eng. Sci. **52**, 4217 (1997).
[11] R. F. Mudde and T. Saito, "Hydrodynamical similarities between bubble column and bubbly pipe flow," J. Fluid Mech. **437**, 203 (2001).
[12] I. M. Mazzitelli and D. Lohse, "Evolution of energy in flow driven by rising bubbles," Phys. Rev. E **79**, 066317 (2009).
[13] G. Riboux, F. Risso, and D. Legendre, "Experimental characterization of the agitation generated by bubbles rising at high Reynolds number," J. Fluid Mech. **643**, 509 (2010).
[14] J. Martinez-Mercado, D. Chehata Gomez, D. Van Gils, C. Sun, and D. Lohse, "On bubble clustering and energy spectra in pseudo-turbulence," J. Fluid Mech. **650**, 287 (2010).
[15] F. Risso, "Theoretical model for k^{-3} spectra in dispersed multiphase flows," Phys. Fluids **23**, 011701 (2011).
[16] Z. Amoura, "Étude hydrodynamique de l'écoulement traversant un réseau aléatoire de sphéres fixes," Ph.D. dissertation, Universite de Toulouse, France, 2008.
[17] D. Seguin, A. Montillet, J. Comiti, and F. Huett, "Experimental characterization of ßow regimes in various porous media-II: Transition to turbulent regime," Chem. Eng. Sci. **53**, 3897 (1998).
[18] D. W. Moore, "The velocity of rise of distorted gas bubbles in a liquid of small viscosity," J. Fluid Mech. **23**, 749 (1965).
[19] H. H. Bruun, *Hot Wire Anemometry: Principles and Signal Analysis* (Oxford University Press, Oxford, UK, 1995).
[20] B. J. Cantwel, "A flying hot-wire study of the turbulent near wake of a circular cylinder at a Reynolds number of 140 000," Ph.D. dissertation, California Institute of Technology, 1976.
[21] D. R. Cole and M. N. Glauser, "Flying hot-wire measurements in an axisymmetric sudden expansion," Exp. Therm. Fluid Sci. **18**, 150 (1998).
[22] G. I. Taylor, "The spectrum of turbulence," Proc. R. Soc. London, Ser. A **164**, 476 (1938).
[23] J. E. Julia, W. K. Harteveld, R. F. Mudde, and H. E. A. Van den Akker, "On the accuracy of the void fraction measurements using optical probes in bubbly flows," Rev. Sci. Instrum. **76**, 035103 (2005).
[24] A. Cartellier and E. Barrau, "Monofiber optical probes for gas detection and gas velocity measurements: optimized sensing tips," Int. J. Multiphase Flow **24**, 1295 (1998).
[25] J. Vejrazka, M. Vecer, S. Orvalho, P. Sechet, M. C. Ruzicka, and A. Cartellier, "Measurement accuracy of a mono-fiber optical probe in a bubbly flow," Int. J. Multiphase Flow **36**, 533 (2010).
[26] P. D. Welch, "The use of fast Fourier transform for the estimation of power spectra: A method based on time averaging over short, modified periodograms," IEEE Trans. Audio Electroacoust. **15**, 70 (1967).
[27] F. A. Mancilla Ramos, "Caracterizacion de un flujo turbulento en la produccion de una emulsion," M.Sc. thesis, Universidad Nacional Autonoma de Mexico, 2009.
[28] H. Tennekes and J. L. Lumley, *A First Course in Turbulence* (The MIT Press, Cambridge, USA, 1972).
[29] S. B. Pope, *Turbulent Flows* (Cambridge University Press, Cambridge, UK, 2000).